Journal of Applied Pharmaceutical Research
Volume 13 Issue 6, Year of Publication 2025, Page 62 – 77
DOI: https://doi.org/10.69857/joapr.v13i6.1478

Check for updates

Research Article

JOURNAL OF APPLIED PHARMACEUTICAL RESEARCH | JOAPR
www.japtronline.com *ISSN: 2348 – 0335*

A NOVEL MUCOADHESIVE NANOFABRICATION STRATEGY FOR LEVOFLOXACIN HEMIHYDRATE OPTIMIZED VIA CENTRAL COMPOSITE DESIGN FOR HELICOBACTER PYLORI THERAPY

R Neelamegarajan[1, 2], N Venkateshwaramurthy[1,2]*, V Senthil[2], K Jaganathan[2], P Manivasakam[2]

Article Information
Received: 2nd August 2025
Revised: 27th October 2025
Accepted: 30th November 2025
Published: 25th December 2025

Keywords
Helicobacter pylori, Levofloxacin hemihydrate, Chitosan, Carbopol 974P, N-Acetylcysteine, Mucoadhesive nanoparticle

ABSTRACT

Background: *Helicobacter pylori* (*H. pylori*), a gram-negative bacterium that causes gastritis, peptic ulcers, and gastric cancer, infects more than half of the global population. The recommended levofloxacin-based nanotherapy can be deployed to overcome rapid gastric emptying of the drug, inadequate drug concentration at the site of action, and the protective mucosal layer. The research established a goal to design and enhance Levofloxacin Hemihydrate Mucoadhesive Nanoparticles (LMNP) for better drug retention on stomach mucosa and mucosal adhesion, site-specific prolonged drug delivery against *H. pylori*. **Methodology:** The LMNP nanoparticles were prepared through ionic gelation of chitosan (CT), carbopol 974P(CP), and N-Acetylcysteine (NAC) before optimizing them using Central Composite Design (CCD) within Response Surface Methodology. The study used FTIR, DSC, XRD, SEM, particle size, zeta potential, entrapment efficiency (EE%), *in vitro* cumulative drug release %, and mucoadhesive strength (MS%) tests for characterization. **Results and Discussion:** The optimized LMNP formulation had a particle size of 245.4 ± 1.254 nm, an EE% of 72 ± 2.246%, and Prolonged drug release over 6 hours with *in vitro* CDR of 99.98 ± 0.115%, which fits the gastric mucus turnover time. FTIR, DSC, and XRD confirmed the compatibility of drug excipients. SEM revealed uniform spherical particles, and MS% was 62 ± 2.315%. The size of the particles and their entrapment efficiency , mucoadhesive properties, and in vitro cumulative drug release were influenced by CT and CP, but NAC enhanced mucopenetration effects. The CCD model successfully established formulation behavior and confirmed synergistic interactions among the excipients. By enhancing matrix formation and swelling, the combined impact of CT and CP significantly influenced. **Conclusion:** The LMNP system developed by employing CCD designs and ionic gelation methodology demonstrated promising characteristics for gastric retention and prolonged drug release , which could enhance *H. pylori* clearance rates. The drug delivery platform presents a practical, biocompatible solution to address challenges in conventional therapy.

[1]*J K K Nattraja College of Pharmacy, Kumarapalayam -638 183, Namakkal District, Tamil Nadu, India.*
[2]*The Tamil Nadu Dr. M.G.R. Medical University,Chennai-600032, India.*

For Correspondence:** **nvmurthy@gmail.com

INTRODUCTION

Helicobacter pylori (*H. pylori*) is a gram-negative bacterium with a spiral structure that changed the science of stomach pathophysiology following its discovery by Barry Marshall and Robin Warren in 1982 [1] Since then, it has been considered one of the most prevalent chronic infections globally, affecting over 50% of the population worldwide who have *H. pylori* [2]. Typically colonized deep within the gastric glands beneath the mucosal layer, producing persistent inflammation of the stomach lining [3]. The infection causes many gastrointestinal diseases, such as peptic ulcers, chronic gastritis, gastric atrophy, mucosa-associated lymphoid tissue (MALT) lymphoma, and adenocarcinoma of the gastric regions [4–7]. Studies suggest that *H. pylori* is involved in over 90% of gastric cancer and MALT lymphoma cases, as well as 80-90% of gastric and duodenal ulcers [8]. Consequently, the International Agency for Research on Cancer (IARC) classifies *H. pylori* as a Group I human carcinogen [9].

Epidemiological data show that a lower prevalence of *H. pylori* cases may lead to less gastric cancer incidence globally [10]. But complete eradication remains challenging due to several factors: rapid gastric emptying of drugs, high acidity, bacterial resistance, low drug concentration at the infection site, and poor treatment adherence resulting from side effects like nausea, vomiting, and altered taste [11–13]. The Maastricht V/Florence Consensus Report reports that levofloxacin-based quadruple therapy (containing a proton pump inhibitor (PPI), levofloxacin, amoxicillin, and bismuth) is recommended as a second-line option following first-line treatment failure. It is also considered a suitable alternative when bismuth-based regimens are unavailable or impractical for clinical use [14]. The American College of Gastroenterology (ACG) recommends a 14-day levofloxacin triple therapy (PPI + levofloxacin 500 mg once a day + amoxicillin 1 g twice a day) as an effective treatment, as a preferred empirical second-line regimen in regions without access to culture and sensitivity testing, especially in areas with known clarithromycin resistance [15].

Recent advances in drug delivery have focused on gastroretentive systems designed to increase local drug concentration and retention time. These systems aim to overcome physiological barriers such as rapid gastric emptying and thick mucus layers [16]. Polymers such as chitosan, Carbopol 974P, and N-acetylcysteine (NAC) have emerged as promising candidates owing to their unique physicochemical properties. Chitosan is a mucoadhesive, biocompatible, and biodegradable polysaccharide with the ability to adhere to gastric mucosa, enhance drug residence, and even disrupt *H. pylori* membranes in acidic environments [17–19]Chitosan protonated amine groups promote strong adhesion and gel formation, mainly when used in combination with Carbopol [20–23]. Carbopol 974P contributes to prolonged gastric residence and controlled release by forming compact, cross-linked gel networks [24–27]. NAC, widely known for its mucolytic and antioxidant properties, disrupts disulfide bonds within the mucus layer, thereby facilitating deeper drug penetration and access to *H. pylori* reservoirs. It also exhibits antimicrobial and antibiofilm effects without cytotoxicity [28–32]. Together, these materials are being integrated into the design of a mucoadhesive nanodrug delivery system for Levofloxacin hemihydrate. Chitosan, Carbopol 974P, and NAC were selected for their synergistic effects on gastric drug delivery. Chitosan exhibits strong mucoadhesive and antimicrobial effects against *H. pylori*, whereas Carbopol 974P forms cross-linked gels that sustain release and prolong gastric retention. NAC exerts a mucolytic effect by disrupting mucus disulfide bonds, thereby enabling deeper penetration into *H. pylori* reservoirs. The novel research work is the strategic combination of chitosan, Carbopol 974P, and NAC into a synergistic dual mucoadhesive–mucopenetrative system coupled with CCD-based optimization, to create an advanced levofloxacin delivery platform tailored for *H. pylori* eradication. And graphically how each polymer influences particle size, drug entrapment, release profile, and mucoadhesion.

MATERIALS AND METHODS

Chitosan (CT) (75% deacetylated) and N-Acetylcysteine (NAC) were purchased from Loba Chemi, Mumbai. Carbopol 974P(CP) was purchased from Yarrow Chem Products, Mumbai. Micro Lab Ltd, Bengaluru, kindly gifted levofloxacin hemihydrate (LH). All other solvents used were HPLC grade.

Experimental design using central composite model (CCD)

CCD, a prominent design in Response Surface Methodology (RSM), was employed to develop a Levofloxacin Hemihydrate mucoadhesive nanoparticle formulation using Design-Expert® (v13.0.9.0) [33–35]. Three factors were varied: chitosan (A), Carbopol 974P (B), and N-acetylcysteine (C) on a total of twenty experimental runs (8 factorial points, 6 axial points, and 6 center points). Table 1 summarizes the experimental limits for each variable. The perfect CCD batches are shown in Table 2. This

model relates the response (Y) to the three independent variables using a second-order polynomial, as shown in Equation 1 [36–38].

$$y = b_0 + \sum_{i=1}^{n} b_i x_i + \sum_{i=1}^{n} b_{ii} x_i^2 + \sum_{i=1}^{n-1} \sum_{j=i+1}^{n} b_{ij} x_i x_j \quad \text{.....(1)}$$

Y is the estimated response, b_0 is the point of intercept (constant coefficient), b_i represents linear coefficients, b_{ii} refers to quadratic coefficients, & b_{ij} represents the interaction coefficients among variables. X_i and X_j represent the coded data of the independent factors. ANOVA was used to assess the statistical significance of each variable ($P < 0.05$), and second-order polynomial terms were included to improve predictive performance. The predicted and interaction effects were illustrated through three-dimensional surface plots and contour diagrams; all data were presented as mean ± SD for at least three replicates.

Study on Drug Excipient Compatibility

The chemical compatibility of levofloxacin hemihydrate with excipients was analyzed using Fourier transform infrared spectroscopy (FTIR), Differential scanning calorimetry (DSC), and X-ray diffraction (XRD).

1. Fourier transform infrared (FTIR) spectroscopy: The pure Levofloxacin Hemihydrate, Polymers, and physical mixtures were analysed using an FTIR spectrophotometer (FTIR- IR Spirit Model, SHIMADZU Corporation, Japan) using the KBr pellet method. A sample (1 mg) was mixed with KBr and made into a disk by applying force in a press. Spectra were recorded in the scan range of 4000-500 cm^{-1} [39–41]

2. Differential scanning calorimetry (DSC): The thermograms of DSC were analysed with the NETZSCH DSC 204 F1 Phoenix using the NETZSCH Proteus software. Levofloxacin hemihydrate exhibited endothermic peaks during melting, typically at 222–231 °C. These peaks represent the melting of the different crystalline forms (a, b, and c forms) of Levofloxacin, as described by the DSC technique, which was used to examine the chemical compatibility of Levofloxacin with various selected excipients[42,43].

3. X-Ray Diffraction (XRD) study: XRD data were obtained using a Smart Lab diffractometer system (Rigaku Corporation, International Marketing Division, Japan) equipped with a CuKα radiation source. During the 60-second data acquisition, the sample was oscillated, and diffraction data were recorded over a 2θ range of 6.822° to 69.536° with a resolution of 0.05°, yielding the diffraction patterns. The sample was positioned on a variable-temperature XYZ stage, and temperature was regulated after a 10-minute equilibration at each set point. Figures 2 and 3 present the XRD patterns of the Levofloxacin Hemihydrate and the physical mixture, respectively [44,45]

4. Design of Levofloxacin Hemihydrate Mucoadhesive Nanoparticles (LMNP): Employing the modified dropping method, with ionic gelation method positively charged chitosan (CT) (75% deacetylated) and negatively charged Carbopol 974P (CP) were combined to develop CT-CP nanoparticles, CT (0.05%, 0.175%, 0.3%, etc., as in Table 1) was mixed in 100 mL of 1% (w/v) of acetic acid to form the CT solution. This solution was then added dropwise to a CP dispersion (0.1%, 0.3%, 0.5%, etc., Table 1) under magnetic stirring for 10 minutes to yield an opalescent suspension, and the pH was adjusted to 4.5 with NaOH. Levofloxacin Hemihydrate Mucoadhesive nanoparticles were prepared by dissolving 1% (w/v) LH in 100 mL of acetone and then adding the drug solution dropwise to the CT-CP mixture while stirring at 1000 rpm for 30 minutes. Simultaneously, a 2% solution of sodium tripolyphosphate was added dropwise. The resulting mixture was sonicated using a KLPRO-500 (KINGLAB) at 500 W and 20 kHz, with a 12 mm probe diameter, for 3, 5, and 10 minutes, at amplitudes of 40, 50, and 60%, respectively. Separately, NAC (107.56, 244.8, and 382.03 mg) was dissolved in 100 mL of ethanol and added dropwise to the nanoparticle dispersion under constant stirring (500 rpm) for 1 hr to form a NAC coating. The final LMNP nanoparticles were lyophilized [46,47].

CHARACTERIZATION OF LEVOFLOXACIN HEMIHYDRATE MUCOADHESIVE NANOPARTICLES

1. Particle size(nm), Zeta potential(ξ) and SEM analysis

The Particle size and Zeta potential analysis were carried out by Dynamic Light Scattering (DLS) of the nanoparticles measured (Table 1) using a Malvern Zetasizer Ver 8.02 (Malvern Instruments Ltd., Worcestershire, UK). The samples were diluted using purified water to the required concentration. Size distribution analysis was performed on 20 runs at 25 °C using clear disposable Zeta cells. For each sample, at least 3 measurements were taken. Results are reported as the mean with standard deviation (SD). SEM morphology was evaluated using a ZEISS Gemini SEM (Germany) at an accelerating voltage of

10 kV, sputter-coated with Au before imaging, and imaged with a secondary electron detector [46–50].

2. Drug Entrapment Efficiency (EE%)

The EE% of the nanoparticles was assessed by isolating the drug-loaded nanoparticles from the aqueous phase containing unbound LH through ultracentrifugation at 10,000 rpm for 30 minutes at 4°C (by Superspin R-V/Fa, Plasto Crafts industries, Mumbai). The amount of LH entrapped within these nanoparticles was calculated by subtracting the amount of drug present in the supernatant from the entire amount of drug used in the dosage form. The concentration of unencapsulated LH in the supernatant was quantified using a validated UV-visible spectrophotometric method (UV-1700 Pharma Spec, SHIMADZU, Japan), assessing the absorbance at 294 nm; each of the measurements was taken in triplicate, and the EE% and Drug content (%) of LH were then calculated using the following Formula (2,3) [51]

$$\mathbf{EE\%} = \frac{\mathbf{Total\ LH - Free\ LH}}{\mathbf{Total\ LH}} \times \mathbf{100} \quad \ldots\ldots\ldots \mathbf{2}$$

$$\mathbf{DC\%} = \frac{\mathbf{Total\ Amount\ of\ Drug\ Used\ in\ Formulation}}{\mathbf{Amount\ of\ Drug\ in\ Nanoparticles}} \mathbf{x100} \ldots \mathbf{3}$$

3. *in vitro* cumulative drug release studies (CDR% in h)

In vitro drug release from LMNP formulations was investigated using a 25 kDa MWCO dialysis membrane in gastric fluid (pH 1.2) at 37 ± 1°C for 12 hours under sink conditions. A suitable amount of nanoparticles was placed in a dialysis tube and immersed in 100 ml of medium, which was continuously stirred on a magnetic stirrer at 37 ± 1°C. At predefined intervals, 1 mL of the diffusion medium was withdrawn and analyzed for drug content using a Shimadzu UV-visible spectrophotometer. To keep the volume and other variables constant, the removed volume was promptly replaced by an equivalent volume of new and warmed medium [52].

4. Mucoadhesive Strength (MS%)

The LMNP mucosal adhesive strengths were tested using an in vitro bioadhesion assay, the wash-off test. A 1 × 1 cm trim of pig gastrointestinal mucosa was attached to a glass slide with an elastic thread. Around 100 mg of LMNP were evenly distributed over the moistened tissue surface. The assembled slide was suspended from one of the notches on a USP tablet disintegration instrument. During the procedure, the tissue was continuously moved up and down in a beaker containing simulated gastric fluid (pH 1.2). At intervals of two hours, 0, 2, 4, and then up to 6 hours, the amount of LMNP still adhered to the tissue surface was recorded [53,54]. The following formula is used to calculate MS%, as shown in Formula 4

$$\mathbf{MS\%} = \left(\frac{\mathbf{Weight\ Remaining\ adhered\ LMNP}}{\mathbf{Weight\ of\ total\ applied\ LMNP}}\right) \times \mathbf{100} \quad \ldots . \mathbf{4}$$

RESULTS AND DISCUSSION

FTIR

Instrumental techniques were used to evaluate compatibility between the drug and excipients. FTIR spectra were recorded for pure Levofloxacin Hemihydrate, each excipient, and physical mixtures (1:1, drug to excipient) as shown in Figure 1. The FTIR spectrum for Levofloxacin Hemihydrate, exhibited absorption bands at 1727.9 cm^{-1} which corresponded to the carboxylic group, 1622.9 cm^{-1} C=N, C=C stretch (aromatic/quinolone), and 2931.1cm^{-1} - 2804.6 cm^{-1} for alkane C–H stretching, 3080.7cm^{-1} for carbonyl group stretching, 1559.7 $^{-1}$ for amine stretching, which provided evidence of the structure and purity of the drug. This study reports no major incompatibility between the drug and the excipients used. The absence of quinolone peaks confirms molecular-level drug-polymer matrix formation: 1541.04 cm^{-1} (N-H bend/aromatic C=C), 1341.22 cm^{-1} (C-N/N-O stretch), 1292.35 cm^{-1} (C-O/C-N stretch), 927.21 cm^{-1} (ring deformation), and 874.02 cm^{-1} (aromatic C-H bend), indicating coordination, restricted mobility, and π-π stacking within the polymer matrix. These specific peaks confirm the entrapment of levofloxacin within the polymer matrix.

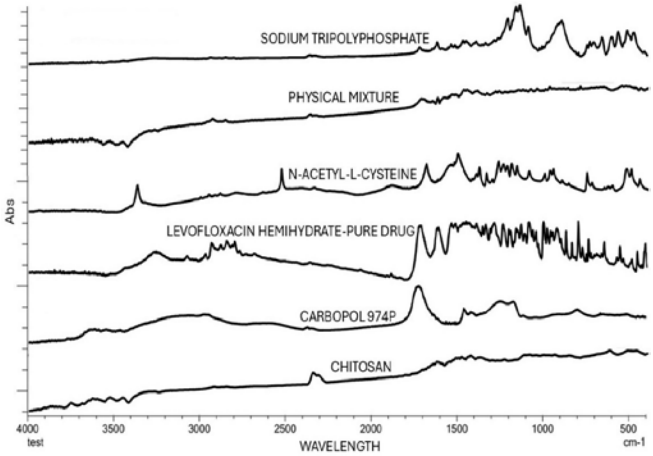

Figure 1: FTIR spectra of Pure Levofloxacin hemihydrate, Physical mixture, and Polymers

XRD: The XRD investigation on both the pure drug and its physical mixture with excipients showed similar peak locations, notably at the characteristic 2θ values of 6.6°, 9.6°, 13.0°, and 19.4°, and no significant shift or new peaks, shown in Figure 2. These findings suggest that there is no chemical interaction between the drug and the excipients in the physical mixture, and that the substance retains its crystalline form.

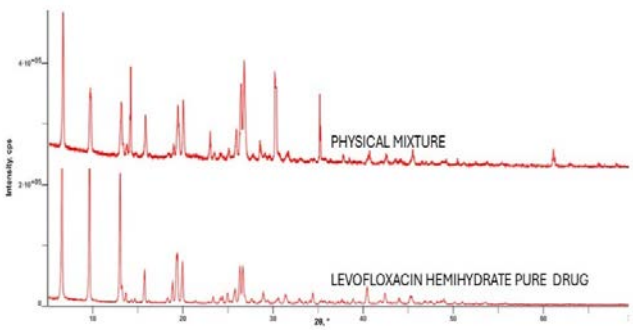

Figure 2: X-ray diffractograms of Pure Levofloxacin hemihydrate, physical mixture

DSC

DSC analysis was performed to determine the chemical compatibility of Levofloxacin and all excipients used. To evaluate thermal behavior, DSC thermograms of pure Levofloxacin and its 1:1 physical mixtures with excipients were obtained, as shown in Figure 3. The thermogram of LH showed a distinct peak at its melting point (229.3 °C). The same peak was measured in all 1:1 w/w drug with excipients physical mixtures at 228.9°C. These results demonstrate that Levofloxacin is chemically stable, as it did not react with the selected excipients during formulation.

Experimental Design:

In this study, we successfully developed Levofloxacin Hemihydrate Mucoadhesive Nanoparticles. Chitosan (A), Carbopol 974P (B), and N-acetylcysteine (C), as summarized in Table 1, were key parameters that significantly affected particle size, entrapment efficiency, cumulative drug release (CDR), and mucoadhesive strength. CCD was selected as the experimental approach for the study, as it is a robust and reliable design that provides accurate results & assessments. A total of twenty experimental runs were conducted using the RSM Central Composite Design (CCD). The combinations of experimental factors produced unique responses that accounted for the influence of each factor on formulation development, as summarized in Table 2.

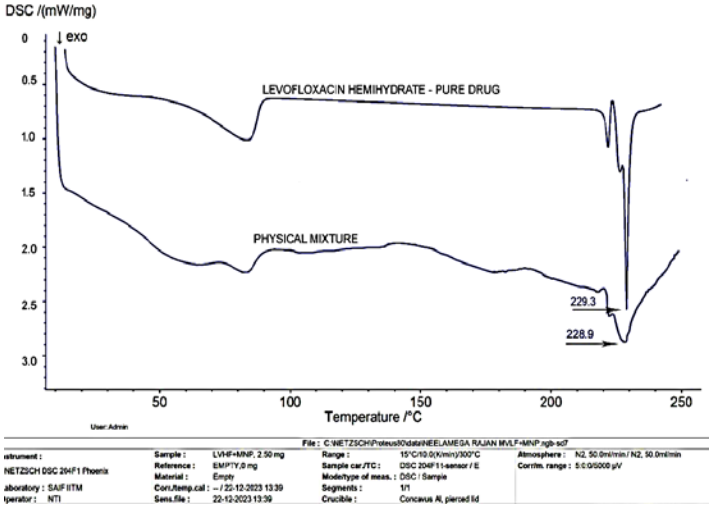

Figure 3. DSC thermograms of Pure Levofloxacin Hemihydrate, Physical mixture

Table 1. Independent variables for CCD experiment design

Independent variable	Levels				
	Low (-1)	Center (0)	High (+1)	-alpha	+alpha
A: Chitosan (%)	0.05	0.175	0.3	-0.0352241	0.385224
B: Carbopol 974P (%)	0.1	0.3	0.5	-0.0363586	0.636359
C: N-Acetylcysteine (NAC) (mg)	107.56	244.8	382.03	13.9942	475.596
Dependent variable					
$Y_{PS\ (nm)}$ = Particle size (nm)					
$Y_{EE\%}$ =Entrapment Efficiency%					
$Y_{CDR\%\ (H)}$ = *in vitro* Cumulative drug release (CDR) (h), Time required to release the drug from the LMNP (Hours)					
$Y_{MS\ (\%)}$ = Mucoadhesion Strength (%)					

Formulation Development of LMNP Nanoparticles

In this study, we synthesized Levofloxacin Hemihydrate mucoadhesive nanoparticles via the ionic gelation method, using chitosan as the mucoadhesive agent & carbopol 974P as the sustained-release polymer. mucopenetration enhancer, in this case, N-Acetylcysteine. Sodium tripolyphosphate (TPP) was also used in the formulation as a cross-linking agent; all agents are biodegradable, nontoxic, and biocompatible. We prepared a total of 20 LMNP formulations (F1-F20) and evaluated particle size, zeta potential, in vitro CDR, Drug entrapment efficiency, and mucoadhesive strength. The pictographic representation of LMNP was shown in Figure 12(C).

Effect of Variables on particle size(nm), Zeta potential(ξ), and SEM morphology

The particle size of the formulated LMNP nanoparticles was measured between 195.0 ± 2.354 nm and 396.4 ± 1.265 nm (Table 2), and the zeta potential ranges from 21.5±1.323 mv to 54.7±0.643 Mv as shown in Figure 4 (B). The most prominent factors contributing to size variation were the concentrations of

chitosan & Carbopol 974P, which exerted positive effects due to increased viscosity & polymer entanglement, particularly when both were present, demonstrating synergistic effects. This was statistically confirmed by the CCD model (R^2 = 0.9596, p = 0.0001, F = 26.40), as shown in Table 3, equation 5. Chitosan (A: +43.9967) & Carbopol (B: +30.5047) were the major contributors & their interaction (AB: +31.5125) further increased the size. In comparison, N-Acetylcysteine (NAC) had a small effect on size, evidenced by a slightly negative linear coefficient (–3.2398) and positive quadratic (C^2: +9.51055) and interaction terms. The sonication parameters (40–60% amplitude) and stirring speed (1000 rpm) affect regulated nucleation during gelation, homogenous stirring of polymeric mixtures, and the shear-triggered fragmentation of large aggregates. The optimal pH of 4.5 promotes stable particle formation, prevents precipitation, promotes partial Carbopol ionization to enhance electrostatic interactions, and enables efficient chitosan protonation (pKa ~ 6.5) for maximal positive charge. This implies that its effect is pronounced only at higher concentrations, in combination with polymers, or with chitosan and Carbopol. It is well established that NAC enhances mucosal penetration; thus, given these properties, it serves well as a modulator with size-enhancing capabilities but is not recognized as a primary size determinant. These findings are corroborated by the contour and 3D plots in Figure 6 (C, D), which indicate that chitosan and Carbopol are the primary determinants of particle size, with NAC serving only as a subtle modulator.

The probability plot further confirmed the model's accuracy, and the residual analysis shown in Figures 6(A, B), which affirms its predictive capabilities and reliability. SEM revealed that the nanoparticles were approximately 180–250 nm in diameter, were globular and rigid, as shown in figures 5(A, B), and a pictorial representation is shown in figure 5(C).

Effect of Variables on Entrapment Efficacy EE%

The EE% of formulated LMNP nanoparticles varied from 42 ± 1.489% to 78 ± 2.365% shown in Table 2 and Figure 7. The chitosan and Carbopol 974P concentrations seemed to be the most important contributors to the EE% and were found to improve drug entrapment because of the synergistic polymeric chitosan-carbopol 974P matrix.EE% was optimal at moderate to high levels of these polymers, while excessive or very low concentrations reduced EE% due to a lack of matrix structure or aggregation. This trend was supported by the CCD model (R^2 = 0.8971, p = 0.0007), where chitosan (A) and Carbopol (B) made strong positive contributions, and their interaction (AB) further enhanced entrapment. But NAC exerted a negligible, nonlinear influence with a minimal positive linear coefficient of 0.8487, AC of 1.5, BC of 0.5, and a negative quadratic C^2 of -2.2770.

Table 2: The CCD batch assigned LMNP formulations and *in vitro* characterization responses

Run	Space Type	Factor 1	Factor 2	Factor 3	Response 1	Response 2	Response 3	Response 4
		A: Chitosan (%)	B: Carbopol 974p (%)	C: N-Acetylcysteine (mg)	Particle Size (mm)	EE (%)	% CDR	Mucoadhesive Strength (%)
1	Center	0.175	0.3	244.795	226.3±3.562	72±2.143	9.66±0.577	62±2.458
2	Factorial	0.05	0.5	107.560	235.0±2.541	58±1.235	4.00±0.000	40±2.365
3	Axial	0.175	0.3	475.596	255.2±3.654	62±2.742	7.33±0.577	65±3.215
4	Factorial	0.3	0.1	382.030	245.4±1.254	72±2.246	6.00±0.000	62±2.315
5	Factorial	0.05	0.1	382.030	202.5±2.345	44±1.874	4.66±0.577	45±1.365
6	Center	0.175	0.3	244.795	235.8±2.148	70±1.263	10.33±0.577	63±1.265
7	Factorial	0.3	0.5	382.030	385.4±3.457	78±2.365	12.00±0.000	82±2.548
8	Axial	-0.0352	0.3	244.795	252.9±2.652	60±2.546	04.33±0.577	20±2.625
9	Factorial	0.05	0.5	382.030	227.2±3.658	64±1.235	7.00±0.000	55±2.246
10	Center	0.175	0.3	244.795	228.4±2.965	68±1.268	9.33±0.577	62±1.987
11	Factorial	0.3	0.1	107.560	248.3±2.457	62±1.689	6.33±0.577	72±2.355
12	Axial	0.175	0.3	013.994	256.0±3.163	67±2.549	8.33±0.577	62±2.165
13	Center	0.175	0.3	244.795	226.8±2.145	74±1.356	10.33±0.577	63±1.452
14	Center	0.175	0.3	244.795	238.4±2.134	72±1.265	10.00±0.00	61±1.326
15	Center	0.175	0.3	244.795	229.3±2.348	71±2.365	9.66±0.577	62±2.785
16	Factorial	0.3	0.5	107.560	396.4±1.265	72±1.548	10.00±0.00	44±2.457
17	Axial	0.3852	0.3	244.795	380.0±1.634	72±2.623	9.00±0.00	83±1.569
18	Axial	0.175	-0.0363	244.795	195.0±2.354	42±1.489	4.33±0.577	16±2.458
19	Factorial	0.05	0.1	107.560	223.7±1.264	46±2.874	4.66±0.577	30±1.548
20	Axial	0.175	0.6363	244.795	250.0±2.165	70±1.326	10.33±0.577	18±1.265

n=3;values are expressed in mean ± SD(Standard Deviation)

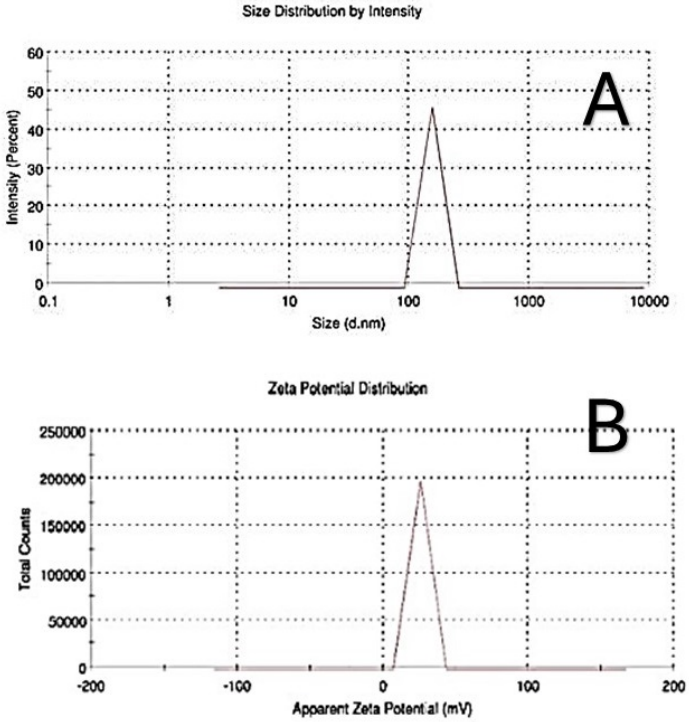

Figure 4: (A) Particle size (nm) of LMNP formulations (B) Zeta potential (mv) of LMNP formulations the positive zetapotential

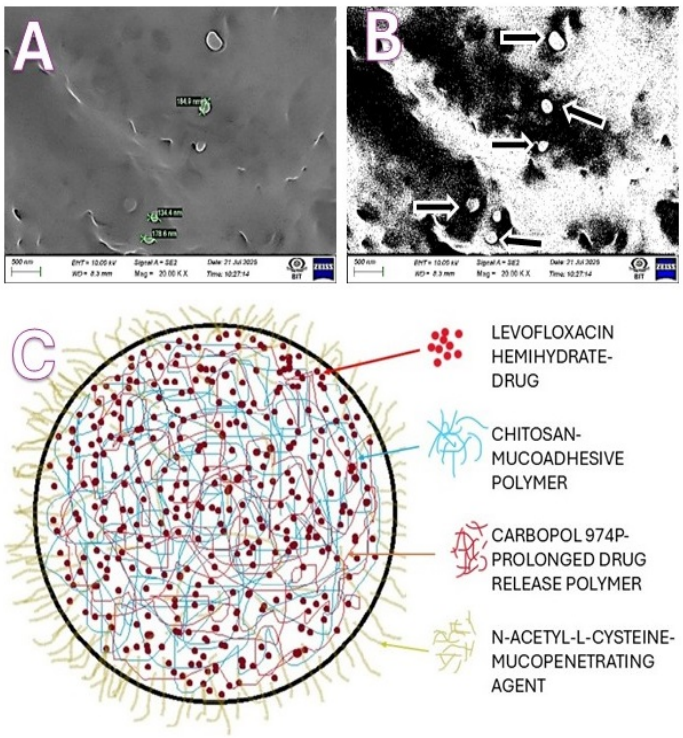

Figure 5: (A) SEM image of LMNP, (B) FE-SEM image shows LMNP, (C) Pictographical representation of LMNP

Table 3: Regression Coefficients and Polynomial Equations for the Response Surface Model

Response	p-value	Fvalue	R^2value	Level of significance	Regression Coefficient equation
$y_{PS(nm)}$	0.0001	26.40	0.9596	***	$y_{PS(nm)} = 230.718 + 43.9967 * A + 30.5047 * \mathrm{B} - 3.2398 * \mathrm{C} + 31.0243 * AB + 1.8875 * \mathrm{AC} + 0.6625 * \mathrm{BC} + 31.0243 * A^2 - 2.19207 * B^2 + 9.51055 * C^2$ **5**
$y_{EE\%}$	0.0007	9.68	0.8971	***	$y_{EE\%} = 71.1544 + 6.74984 * A + 6.96282 * \mathrm{B} - 0.848734 * \mathrm{C} - 2 * AB + 1.5 * AC + 0.5 * BC - 1.74666 * A^2 - 5.28219 * B^2 + 2.27699 * C^2$ **6**
$y_{CDR\,\%}$	0.0001	27.87	0.9617	***	$y_{CDR\%(H)} = 9.67355 + 1.71408 * A + 1.69078 * \mathrm{B} + 0.24297 * \mathrm{C} + 0.875 * AB - 0.125 * AC + 0.625 * BC - 1.16458 * A^2 - 0.987808 * B^2 - 0.811031 * C^2$ **7**
$y_{MS\%}$	0.0024	7.250	0.8671	*	$y_{MS\%} = 61.8163 + 14.3483 * A + 1.12497 * \mathrm{B} + 4.61639 * \mathrm{C} - 3.5 * AB - 0.25 * AC + 6 * BC - 1.4812 * A^2 - 13.6788 * B^2 + 2.76144 * C^2$ **8**

Level of significance : p < 0.05, *p < 0.01, **p < 0.001

This suggests moderate NAC levels aid EE%, whereas extremes disrupt the matrix. NAC likely acts in a modulatory capacity, stabilizing the system rather than as a primary determinant.

The 2D contour and 3D surface plots are shown in Figure 8 (C, D). Those effects are evident, with peak EE% occurring within an optimal range of chitosan and Carbopol concentrations, and subtler contributions from NAC. Residual analyses confirmed the model's reliability, demonstrating good fit and predictive accuracy. The entrapment efficiency behavior can be described mathematically using a quadratic regression model shown in Table 3, equation 6.

The above finding illustrates how chitosan and Carbopol 974P contribute positively and synergistically to entrapment efficiency. In contrast, diminishing returns at higher concentrations are captured by negative quadratic terms, and the smaller NAC coefficients further affirm their role as secondary modulators. Because a thicker, cross-linked matrix forms that retains the drug and inhibits its diffusion, EE% increases with

increasing polymer concentration. Electrostatic interactions with the polymers strengthen the matrix, whereas drug release decreases with increased viscosity. By reducing the drug's surface interaction, the larger particle size generated by this technique further enhances trapping.

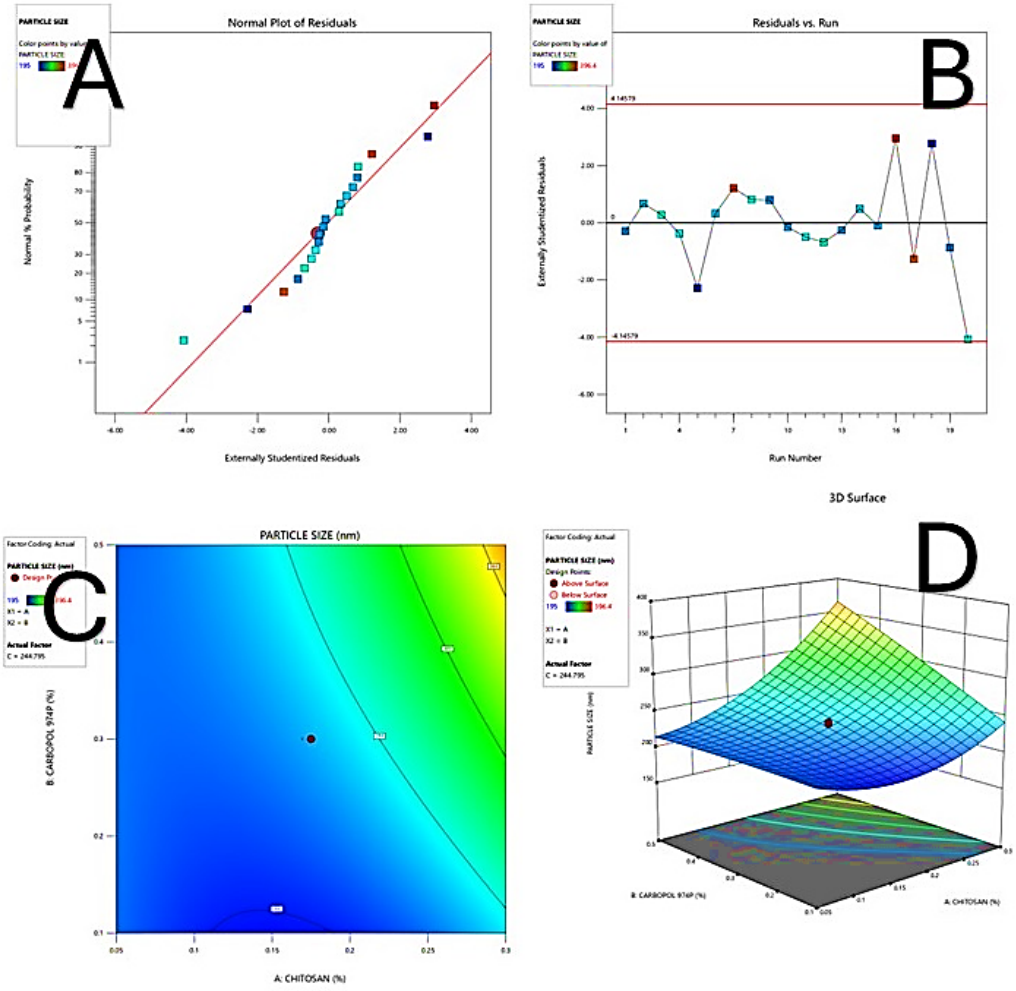

Figure 6: (A) Normal Probability Plot of particle size, (B) Residuals vs Run plot of particle size, (C) 2D- Response surface diagrams of the impact of carbopol and chitosan on particle size, (D) 3D- Response surface diagrams of the impact of carbopol and chitosan on particle size

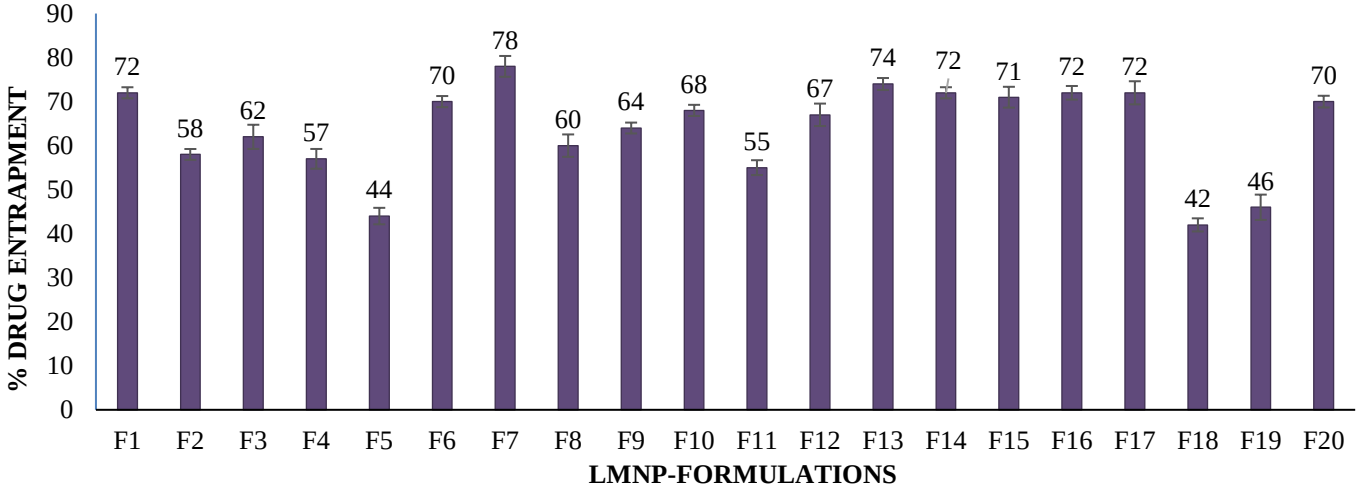

n=3;values are expressed in mean ± SD (Standard Deviation)

Figure 7: Drug Entrapment Percentage vs LMNP Formulations: Comparison chart of drug Entrapment Efficiency % of 1 to 20 LMNP formulations

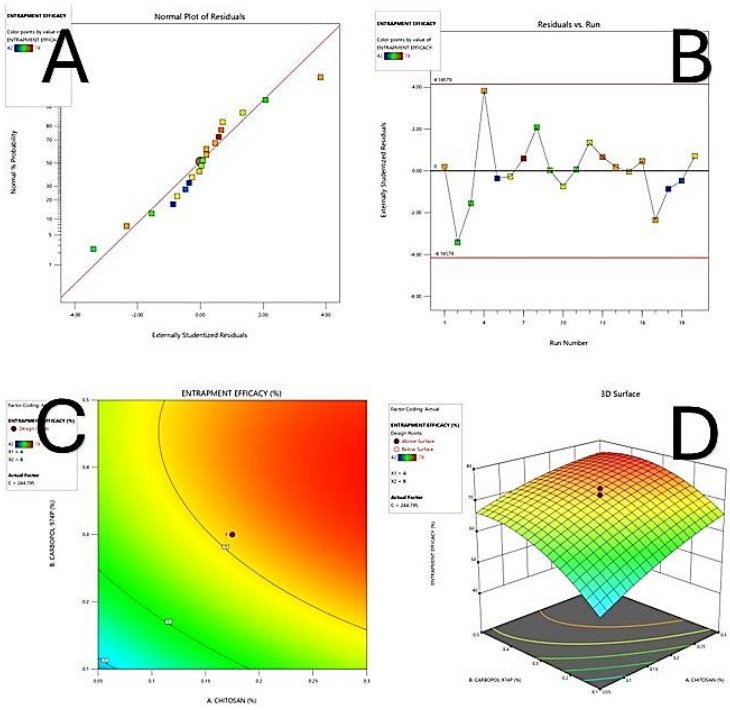

Figure 8: (A) Normal Probability Plot of Drug entrapment efficiency (EE%), (B) Residuals vs Run plot of EE%, (C) 2D-Response surface diagrams of the impact of carbopol and chitosan on EE%, (D) 3D- Response surface diagrams of the impact of carbopol and chitosan on EE%

Effect of Variables on cumulative drug release (CDR%)

The CDR ranges were 04.33±0.577-12.00±0.000 h, as shown in Table 2. All 20 LMNP formulations in vitro CDR% are shown in Figure 9(A, B, C, D). The cumulative drug release behavior can be described mathematically using a quadratic regression model shown in Table 3 equation 7 (P= 0.0001; F = 27.87; R^2 = 0.9617), showed that chitosan (A) and Carbopol 974P (B) both had a significant and similar effect in extending release time as they both enhanced swelling of the matrices and gel formation NAC (C) provided a limited but pronounced hydrophilic disruption of the matrix that allowed a sustained-release pattern.

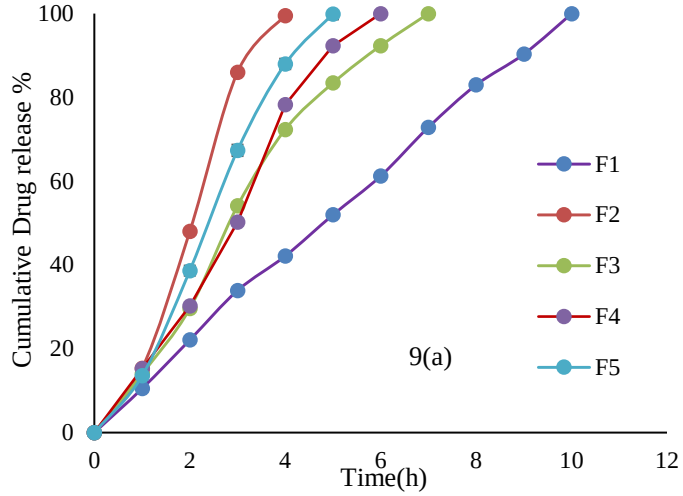

n=3;values are expressed in mean ± SD(standard deviation)

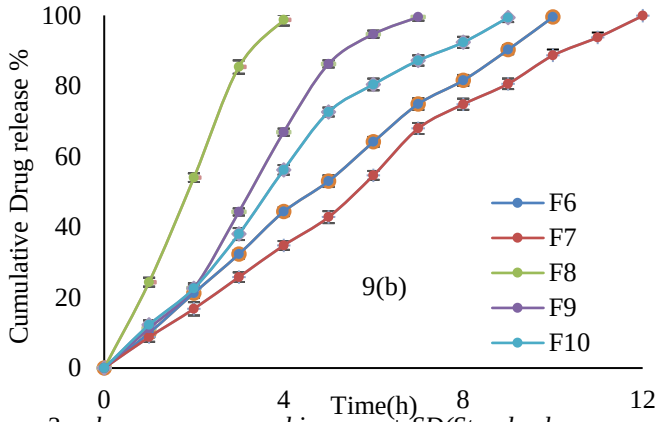

n=3;values are expressed in mean ± SD(Standard

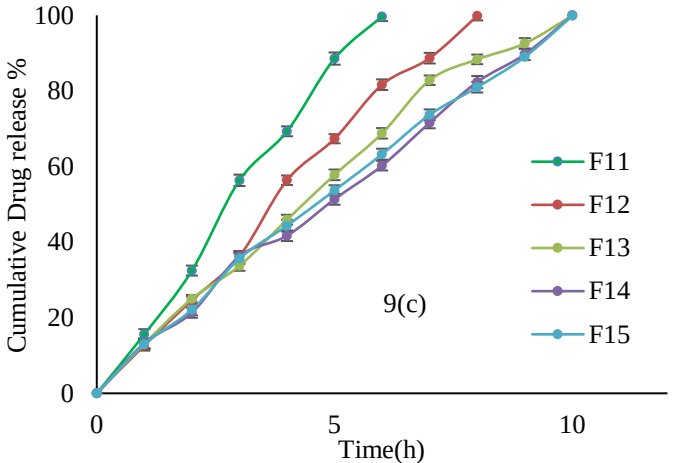

n=3;values are expressed in mean ± SD(standard deviation)

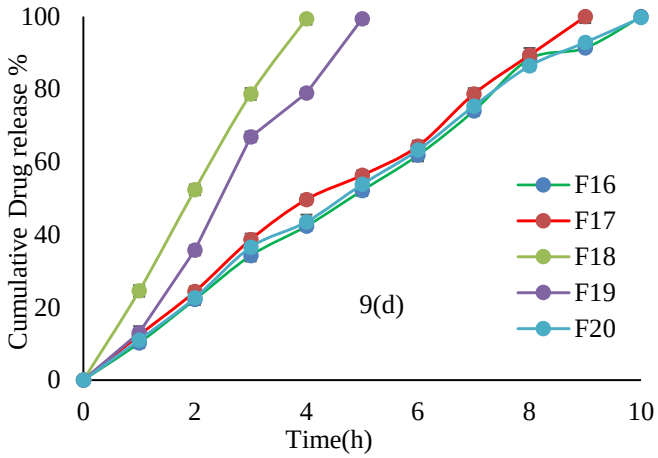

n=3;values are expressed in mean ± SD(Standard Deviation)

Figure 9. *In vitro* cumulative drug release % for LMNP formulations at pH 1.2 (A)LMNP F1 TO F5 (B)LMNP F6 TO F10 (C)LMNP F11 TO F15(D)LMNP F16TO F20

The positive interaction term of chitosan and Carbopol 974P (+0.875) indicated that polyelectrolyte complexes formed synergistically with chitosan and Carbopol 974P, which, along with matrix density, slowed the diffusion properties of drugs.

The negative quadratic terms were assumed to indicate that high concentrations of the polymers or NAC would be less effective due to over-crosslinking or excessive matrix densification. The normal probability and residuals-versus-run graphs shown in Figure 10 (A, B) confirmed appropriate modeling, while the 2D contour and 3D plots shown in Figure 10 (C, D) indicated that the ideal mid-range polymer concentrations were based on desired sustained-release disengagement, with NAC acting as a secondary modulator.

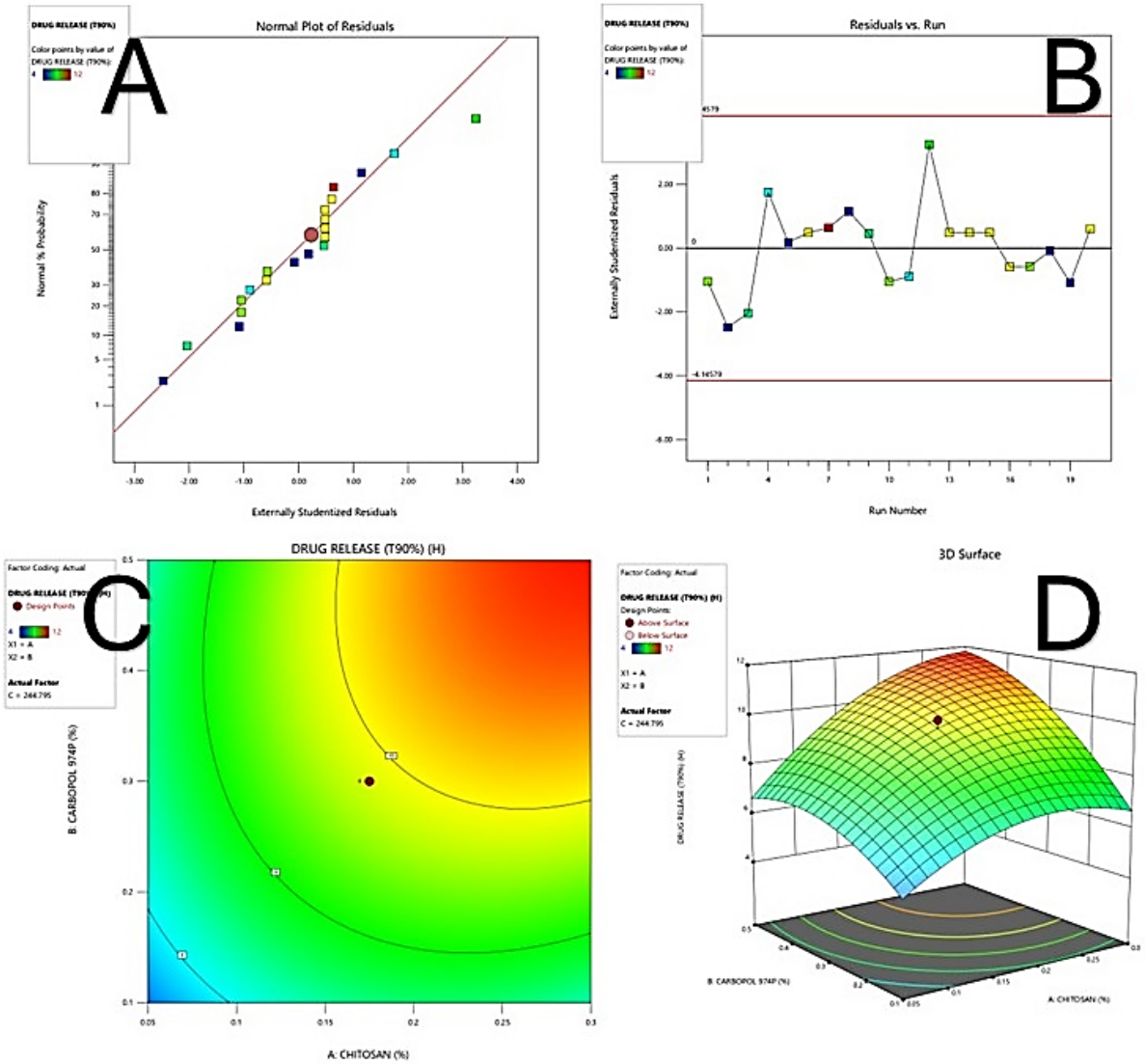

Figure 10: (A) Normal Probability Plot of *in vitro* Cumulative Drug Release % (CDR) in hours, (B) Residuals vs Run plot of CDR, (C) 2D- Response surface diagrams of the impact of carbopol and chitosan on CDR, (D)3D- Response surface diagrams of the impact of carbopol and chitosan on CDR%

Kinetic study

Table 4: Kinetic study data of the best fit formulation: LMNP-Run 04

Time (Hr)	cumulative % DR	% drug remaining	Square root time	log Cumu % drug remaining	log time	log Cumu % DR	% DR	Cube Root of % drug Remaining(Wt)	Wo-Wt
0	0	100	0.000	2.000	0.00	0.000	100	4.642	0.000
1	15.22	84.78	1.000	1.928	0.00	1.182	15.22	4.393	0.249
2	30.21	69.79	1.414	1.844	0.30	1.480	14.99	4.117	0.525
3	50.26	49.74	1.732	1.697	0.47	1.701	20.05	3.678	0.964
4	78.23	21.77	2.000	1.338	0.60	1.893	27.97	2.792	1.850
5	92.35	7.65	2.236	0.884	0.69	1.965	14.12	1.970	2.672
6	99.98	0.02	2.449	-1.699	0.77	2.000	7.63	0.271	4.371

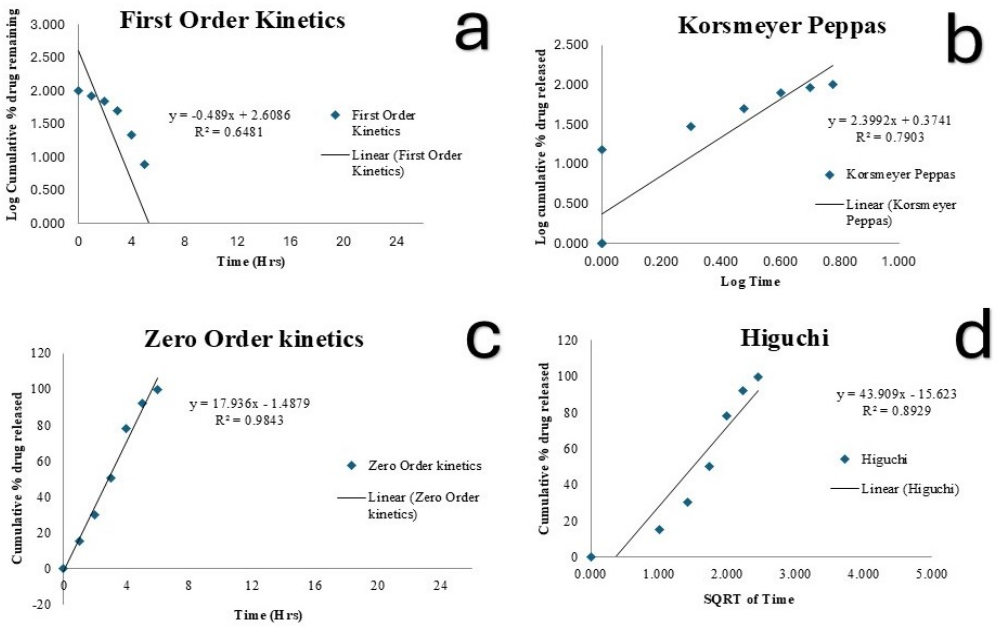

Figure 13: (a) First order kinetics, (b) Korsmeyer Peppas, (c) Zero order kinetics, (d) Higuchi

Zero-order, first-order, Higuchi, and Korsmeyer-Peppas models [55–58] were used to analyze drug release kinetics. Distinct patterns, with varying degrees of association, were observed in the analysis of the release data. The best-fit LMNP 04 was obtained using the zero-order model (R2 = 0.9843; y = 17.936x – 1.4879), indicating a constant release rate independent of concentration. However, the lowest correlation was observed in the first-order model (R2 = 0.6481; y = -0.489x + 2.6086). The LMNP formulation may exhibit a multi-mechanism drug-release profile, consisting of a zero-order initial drug-burst phase followed by an erosion-diffusion phase. The Higuchi model further confirmed diffusion-controlled drug release from the matrix, showing high agreement (R2 = 0.8929; y = 43.909x – 15.623).

The release exponent (≈ 1.1) indicates that drug release is predominantly governed by polymer relaxation, swelling, and structural erosion, which was significantly higher than the 0.89 threshold for anomalous non-Fickian diffusion, and the Korsmeyer-Peppas model showed acceptable correlation (R2=0.7903; y=2.392x+0.3741). The zero-order, Higuchi, Korsmeyer-Peppas, first-order was the sequence of fitting the model shown in the Figure 13 (a,b,c,d), showing that polymer swelling, relaxation, and erosion play a significant role in drug release, initially drug release may controlled by zero-order kinetics followed by polymer swelling, relaxation, and erosion

Effect of variables on mucoadhesion strength (MS%)

A minimum of 16±2.458% and a maximum of 83±1.569% were associated with MS%, as shown in Figure 11. The model derived from CCD-Chitosan (A) most effectively improves mucoadhesion through electrostatic and hydrogen bonding with mucin glycoproteins, while Carbopol 974P (B) makes a minor contribution by increasing polymer-mucin contact through swelling (P = 0.0024; F = 7.25; R2 = 0.8671).

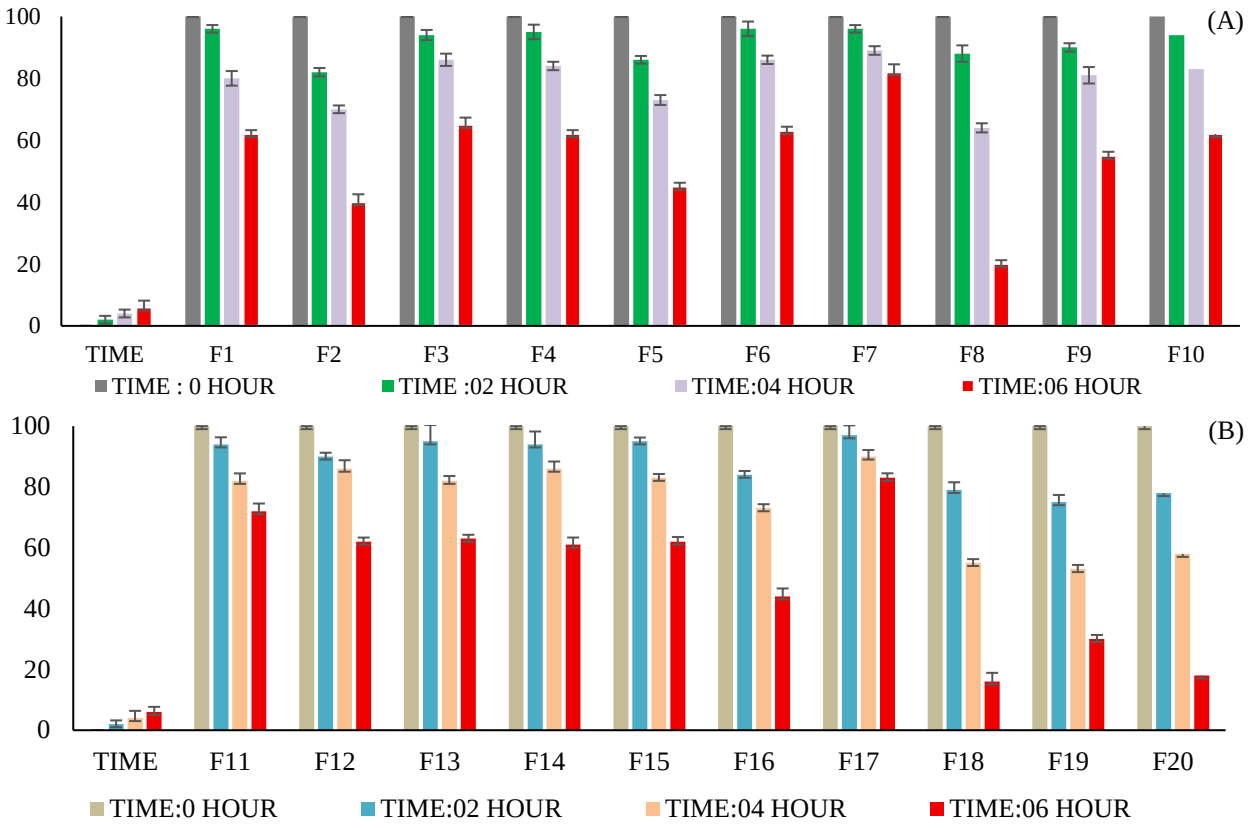

n=3;values are expressed in mean ± SD(Standard Deviation)

Figure 11: Mucoadhesive strength (%) of LMNP Formulations (A)F1 TO F10 (B) F11 TO 20

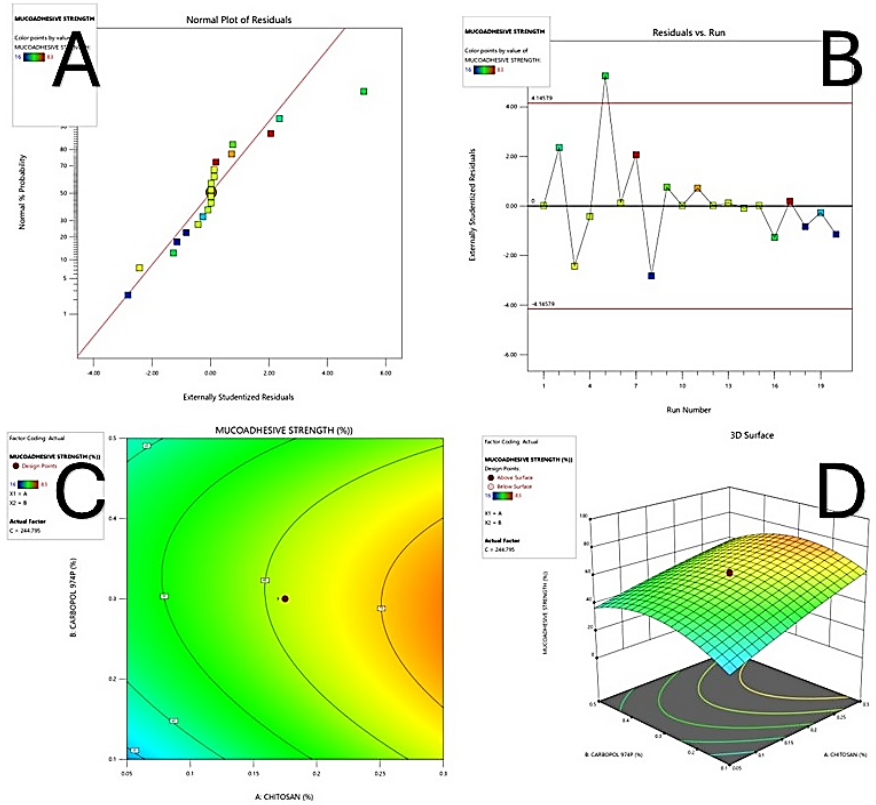

Figure 12. (A) Normal Probability Plot of Mucoadhesive Capacity %(MC%) of LMNP formulation (B) Residuals vs Run plot of MC% (C) 2D- Response surface diagrams of the impact of carbopol974 P and chitosan on MC% (D) 3D- Response surface diagrams of the effects of carbopol and chitosan on MS%

By promoting thiol-mediated mucin crosslinking and polymer flexibility, N-acetylcysteine (C) contributes a secondary beneficial effect. The strong negative quadratic term for B2 (-13.68) and the negative AB interaction (-3.5) shown in Table 3, Equation 8, indicate that excessive polymer levels reduce adhesion due to steric hindrance and over-crosslinking. Plots of residuals versus runs and normal probability in verification.

The model's validity is confirmed by the normal probability and residuals vs. run plots shown in Figure 12(A, B), while the 2D Contour and 3D surface plots shown in Figure 12(C, D) indicate the optimal region for maximum mucoadhesive strength at high chitosan, moderate Carbopol, and moderate NAC. Due to its protonated amino groups, strong electrostatic bonds with negatively charged mucin glycoproteins, and the extensive hydrogen bonding between its hydroxyl and amino functionalities and its carboxyl and hydroxyl sites, chitosan has a superior positive effect on mucoadhesive strength. Mucus mesh is penetrated and entangled by flexible chitosan chains, which produce mechanical interlocking that withstands shear stresses. Chitosan, the most significant positive coefficient in the CCD, is explained by these synergistic effects.

$$\boldsymbol{MS\%} = \left(\frac{\boldsymbol{Weight\ Remaining\ adhered\ LMNP}}{\boldsymbol{Weight\ of\ total\ applied\ LMNP}}\right) \times \mathbf{100} \ldots . \mathbf{4}$$

CONCLUSION

Levofloxacin Hemihydrate Mucoadhesive Nanoparticles (LMNP 20 formulations) were developed in this study using the ionic gelation method with a CCD model. Particle size of 245.4±1.254 nm, Entrapment Efficiency of 72±2.246%, *in vitro* cumulative drug release 99.98 ± 0.115% about 6 hours, suited with stomach mucus turnover time, kinetic study showed multi-mechanistic release profile, with diffusion and erosion-controlled mechanisms, and Mucoadhesive Strength of 62±2.315% were among the encouraging features of the optimized formulation. By enhancing matrix formation and swelling, the combined effects of chitosan and Carbopol 974P significantly influenced drug encapsulation, mucoadhesion, and particle size. N-acetylcysteine (NAC) enhanced mucosal penetration into the stomach. The enhanced LMNP formulation was used as an efficient delivery system to eradicate *H. pylori* because it demonstrated strong adherence to the gastric mucosa and prolonged drug release. The results of this study align with in vivo models, suggesting that this strategy may improve clinical outcomes and treatment efficacy in *H. pylori* infections.

FINANCIAL ASSISTANCE

NIL

CONFLICT OF INTEREST

The authors declare no conflict of interest.

AUTHOR CONTRIBUTION

R. Neelamegarajan conceptualized the article's original idea. N. Venkateswaramurthy and V. Senthil performed the literature review. P. Manivasakam and K. Jaganathan contributed to the data compilation and manuscript preparation. All the activities were done under the guidance and supervision of N. Venkateswaramurthy.

REFERENCE

[1] Yi M, Chen S, Yi X, Zhang F, Zhou X, Zeng M, Song H. Helicobacter pylori infection process: from the molecular world to clinical treatment. *Front. Microbiol.*, **16**, 1541140 (2025) https://doi.org/10.3389/fmicb.2025.1541140

[2] Siddiqui MAM, Siddiqui MMR. 38 years journey of Helicobacter pylori: where it is now? *J. Bangladesh Coll. Phys. Surg.*, **38**(**2**), 53–55 (2020) https://doi.org/10.3329/jbcps.v38i2.45627

[3] Malfertheiner P, Camargo MC, El-Omar E, Liou JM, Peek R, Schulz C, Smith SI, Suerbaum S. Helicobacter pylori infection. *Nat. Rev. Dis. Primers*, **9**(**1**), 19 (2023) https://doi.org/10.1038/s41572-023-00431-8

[4] Liou JM, Malfertheiner P, Lee YC, Sheu BS, Sugano K, Cheng HC et al. Screening and eradication of Helicobacter pylori for gastric cancer prevention: the Taipei global consensus. *Gut*, **69**(**12**), 2093–112 (2020) https://doi.org/10.1136/gutjnl-2020-322368

[5] Matysiak-Budnik T, Priadko K, Bossard C, Chapelle N, Ruskoné-Fourmestraux A. Clinical management of patients with gastric MALT lymphoma: a gastroenterologist's point of view. *Cancers*, **15**(**15**), 3811 (2023) https://doi.org/10.3390/cancers15153811

[6] Lima de Souza Gonçalves V, Cordeiro Santos ML, Silva Luz M, Santos Marques H, de Brito BB, França da Silva FA, Souza CL, Oliveira MV, de Melo FF. From Helicobacter pylori infection to gastric cancer: current evidence on the immune response. *World J. Clin. Oncol.*, **13**(**3**), 186–99 (2022) https://doi.org/10.5306/wjco.v13.i3.186

[7] Seeger AY, Ringling MD, Zohair H, Blanke SR. Risk factors associated with gastric malignancy during chronic Helicobacter pylori infection. *Med. Res. Arch.*, **8**, 1–20 (2020) https://doi.org/10.18103/mra.v8i3.2068

[8] Shatila M, Thomas AS. Current and future perspectives in the diagnosis and management of Helicobacter pylori infection. *J.*

Clin. Med., **11**(**17**), 5086 (2022) https://doi.org/10.3390/jcm11175086

[9] Park JY, Georges D, Alberts CJ. Global lifetime estimates of expected and preventable gastric cancers across 185 countries. *Nat. Med.*, **31**, 3020–7 (2025) https://doi.org/10.1038/s41591-025-03793-6

[10] Chen YC, Malfertheiner P, Yu HT, Kuo CL, Chang YY, Meng FT. Global prevalence of Helicobacter pylori infection and incidence of gastric cancer between 1980 and 2022. *Gastroenterology*, **166**(**4**), 605–19 (2024) https://doi.org/10.1053/j.gastro.2023.12.022

[11] Ali A, AlHussaini KI. Helicobacter pylori: a contemporary perspective on pathogenesis, diagnosis and treatment strategies. *Microorganisms*, **12**(**1**), 222 (2024) https://doi.org/10.3390/microorganisms12010222

[12] Azrad M, Vazana D, On A, Paritski M, Rohana H, Roshrosh H, Agay-Shay K, Peretz A. Antibiotic resistance patterns of Helicobacter pylori in North Israel – a six-year study. *Helicobacter*, **27**(**6**), e12932 (2022) https://doi.org/10.1111/hel.12932

[13] Li B, Lan X, Wang L, Zhao J, Ding J, Ding H, Lei J, Wei Y, Zhang W. Proton-pump inhibitor and amoxicillin-based triple therapy containing clarithromycin versus metronidazole for Helicobacter pylori: a meta-analysis. *Microb. Pathog.*, **142**, 104075 (2020) https://doi.org/10.1016/j.micpath.2020.104075

[14] Jukic I, Vukovic J, Rusic D, Bozic J, Bukic J, Leskur D, Perisin AS, Modun D. Adherence to Maastricht V/Florence consensus report for the management of Helicobacter pylori infection among primary care physicians and medical students in Croatia: a cross-sectional study. *Helicobacter*, **26**(**2**), e12775 (2020) https://doi.org/10.1111/hel.12775

[15] Chey WD, Howden CW, Moss SF, Morgan DR, Greer KB, Grover S, Shah SC. ACG clinical guideline: treatment of Helicobacter pylori infection. *Am. J. Gastroenterol.*, **119**(**9**), 1730–53 (2024) https://doi.org/10.14309/ajg.0000000000002968

[16] Lai Y, Wei W, Du Y, Gao J, Li Z. Biomaterials for Helicobacter pylori therapy: therapeutic potential and future perspectives. *Gut Microbes*, **14**(**1**), 2120747 (2022) https://doi.org/10.1080/19490976.2022.2120747

[17] Ke CL, Deng FS, Chuang CY, Lin CH. Antimicrobial actions and applications of chitosan. *Polymers*, **13**, 904 (2021) https://doi.org/10.3390/polym13060904

[18] Chang SH, Hsieh PL, Tsai GJ. Chitosan inhibits Helicobacter pylori growth and urease production. *Mar. Drugs*, **18**(**11**), 542 (2020) https://doi.org/10.3390/md18110542

[19] Tolaimate A, Desbrières J, Rhazi M, Alagui A, Vincendon M, Vottero P. On the influence of deacetylation process on the physicochemical characteristics of chitosan from squid chitin. *Polymer*, **41**(**7**), 2463–9 (2000) https://doi.org/10.1016/S0032-3861(99)00400-0

[20] Tan Q, Kan Y, Huang H, Wu W, Lu X. Probing the molecular interactions of chitosan films in acidic solutions with different salt ions. *Coatings*, **10**(**11**), 1052 (2020) https://doi.org/10.3390/coatings10111052

[21] Ways TMM, Filippov SK, Maji S, Glassner M, Cegłowski M, Hoogenboom R, King S, Lau WM, Khutoryanskiy VV. Mucus-penetrating nanoparticles based on chitosan grafted with various non-ionic polymers: synthesis, structural characterisation and diffusion studies. *J. Colloid Interface Sci.*, **626**, 251–64 (2022) https://doi.org/10.1016/j.jcis.2022.06.126

[22] Rehman S, Jamil QA, Noreen S, Ashraf MA, Madni A, Mahmood H, Shoukat H, Raza MR. Preparation and evaluation of pH-sensitive chitosan/alginate nanohybrid mucoadhesive hydrogel beads: an effective approach to a gastro-retentive drug delivery system. *Pharmaceutics*, **16**(**11**), 1451 (2024) https://doi.org/10.3390/pharmaceutics16111451

[23] Raj Kumar, Tamanna Islam, Md Nurunnabi. Mucoadhesive carriers for oral drug delivery. *J. Control. Release*, **351**, 504–59 (2022) https://doi.org/10.1016/j.jconrel.2022.09.024

[24] Migliozzi S, Meridiano G, Angeli P, Mazzei L. Investigation of the swollen state of Carbopol molecules in non-aqueous solvents through rheological characterization. *Soft Matter*, **16**(**33**), 7742–55 (2020) https://doi.org/10.1039/d0sm01196g

[25] Kaur M, Sharma A, Puri V, Aggarwal G, Maman P, Huanbutta K, Nagpal M, Sangnim T. Chitosan-based polymer blends for drug delivery systems. *Polymers*, **15**(**9**), 2028 (2023) https://doi.org/10.3390/polym15092028

[26] Gökçe G, Karavana SY, Bağriyanik A, Pekçetin C, Algin Yapar E, Aybar Tural G, Gökçe EH. Design and in vitro, in vivo evaluation of antioxidant bioadhesive gels for burn treatment. *Turk. J. Biol.*, **46**(**3**), 251–62 (2022) https://doi.org/10.55730/1300-0152.2613

[27] Mashabela LT, Maboa MM, Miya NF, Ajayi TO, Chasara RS, Milne M, Mokhele S, Demana PH, Witika BA, Siwe-Noundou X, Poka MS. A comprehensive review of cross-linked gels as vehicles for drug delivery to treat central nervous system disorders. *Gels*, **8**(**9**), 563 (2022) https://doi.org/10.3390/gels8090563

[28] Manoharan A, Ognenovska S, Paino D, Whiteley G, Glasbey T, Kriel FH, Farrell J, Moore KH, Manos J, Das T. N-acetylcysteine protects bladder epithelial cells from bacterial invasion and displays antibiofilm activity against urinary tract bacterial pathogens. *Antibiotics*, **10**(**8**), 900 (2021) https://doi.org/10.3390/antibiotics10080900

[29] Pinto RM, Monteiro C, Costa Lima SA, Casal S, Van Dijck P, Martins MCL, Nunes C, Reis S. N-acetyl-L-cysteine-loaded nanosystems as a promising therapeutic approach toward the eradication of *Pseudomonas aeruginosa* biofilms. *ACS Appl. Mater. Interfaces*, **13**(**36**), 42329–43 (2021) https://doi.org/10.1021/acsami.1c05124

[30] Tenório MCS, Graciliano NG, Moura FA, Oliveira ACM, Goulart MOF. N-acetylcysteine (NAC): impacts on human health. *Antioxidants*, **10**, 967 (2021) https://doi.org/10.3390/antiox10060967

[31] Pedre B, Barayeu U, Ezeriņa D, Dick TP. Mechanism of NAC: role of H_2S and sulfane sulfur. *Pharmacol. Ther.*, **228**, 107916 (2021) https://doi.org/10.1016/j.pharmthera.2021.107916

[32] Taipaleenmäki E, Städler B. Recent advancements in using polymers for intestinal mucoadhesion and mucopenetration. *Macromol. Biosci.*, **20**(**3**), e1900342 (2020) https://doi.org/10.1002/mabi.201900342

[33] Reji M, Kumar R. Response surface methodology (RSM): an overview to analyze multivariate data. *Indian J. Microbiol. Res.*, **9**(**4**), 241–8 (2022) https://doi.org/10.18231/j.ijmr.2022.042

[34] Hassan H, Adam SK, Alias E, Meor Mohd Affandi MMR, Shamsuddin AF, Basir R. Central composite design for formulation and optimization of solid lipid nanoparticles to enhance oral bioavailability of acyclovir. *Molecules*, **26**(**18**), 5432 (2021) https://doi.org/10.3390/molecules26185432

[35] Alam P, Shakeel F, Foudah AI, Alshehri S, Salfi R, Alqarni MH, et al. Central composite design (CCD) for the optimisation of ethosomal gel formulation of *Punica granatum* extract: in vitro and in vivo evaluations. *Gels*, **8**(**8**), 511 (2022) https://doi.org/10.3390/gels8080511

[36] Rathee S, Ojha A, Singh KR, Arora VK, Prabhakar PK, Agnihotri S, et al. Revolutionizing goat milk gels: a central composite design approach for synthesizing ascorbic acid functionalized iron oxide nanoparticles decorated alginate chitosan nanoparticles fortified smart gels. *Heliyon*, **9**(**9**), e19890 (2023) https://doi.org/10.1016/j.heliyon.2023.e19890

[37] Szpisják-Gulyás N, Al-Tayawi AN, Horváth ZH, László Z, Kertész S, Hodúr C. Methods for experimental design, central composite design and the Box–Behnken design, to optimise operational parameters: a review. *Period. Polytech. Chem. Eng.*, **67**(**4**), 521–37 (2023) https://doi.org/10.1556/066.2023.00235

[38] Zamora Lagos SI, Murillo Salas J, Valencia Zapata ME, Mina Hernández JH, Grande Tovar CD. Optimization by central composite experimental design of the synthesis of physically crosslinked chitosan spheres. *Biomimetics*, **5**(**4**), 63 (2020) https://doi.org/10.3390/biomimetics5040063

[39] Arshad MS, Kiran M, Mudassir J, Farhan M, Hussain A, Abbas N. Formulation, optimization, in vitro and in vivo evaluation of levofloxacin hemihydrate floating tablets. *Braz. J. Pharm. Sci.*, **58**, e18630 (2022) https://doi.org/10.1590/s2175-97902022e18630

[40] Numan RS, Abdoon FM. Utility of silver nanoparticles as coloring sensor for determination of levofloxacin in its pure form and pharmaceutical formulations using spectrophotometric technique. *AIP Conf. Proc.*, **2213**, 020103 (2020) https://doi.org/10.1063/5.0000235

[41] Sabei FY, Safhi AY, Alsalhi A, Khan KA, Bakkari MA, Al Fatease A. Preparation and in vitro evaluation of levofloxacin-loaded floating tablets using various rate-controlling agents. *ACS Omega*, **8**(**45**), 42659–66 (2023) https://doi.org/10.1021/acsomega.3c05419

[42] Nugrahani I, Nuur Aini AF, Wibowo MS. Solid-state properties and antibiotic potency of levofloxacin-dicarboxylate salts prepared by the green method. *Heliyon*, **10**(**22**), e40373 (2024) https://doi.org/10.1016/j.heliyon.2024.e40373

[43] Saxena GK, Tiwari R. Design, development and characterization of gastroretentive floating tablet of levofloxacin using natural polymer peanut husk. *Int. J. Drug Deliv. Technol.*, **14**(**3**), 1404–7 (2024) https://doi.org/10.25258/ijddt.14.3.22

[44] Kadri L, Carta M, Lampronti G, Delogu F, Tajber L. Solvent-induced crystal polymorphism in liquid crystal systems: characterization and phase transformation. *Mol. Pharm.*, **21**(**6**), 2838–53 (2024) https://doi.org/10.1021/acs.molpharmaceut.4c00188

[45] Wei N, Jia L, Shang Z, Gong J, Wu S, Wang J, et al. Polymorphism of levofloxacin: structure, properties and phase transformation. *CrystEngComm*, **21**(**36**), 5452–62 (2019) https://doi.org/10.1039/C9CE00656B

[46] Mohamed S, Nasr M, Refai H. Preparation and characterization of terbutaline sulphate-loaded chitosan/Carbopol nanoparticles. *Int. J. Pharm. Sci. Drug Res.*, **3**(**1**), 30–4 (2019) https://doi.org/10.21608/APRH.2019.6474.1071

[47] Ruiz Pulido G, Quintanar Guerrero D, Serrano Mora LE, Medina DI. Triborheological analysis of reconstituted gastrointestinal mucus/chitosan: TPP nanoparticles system to study mucoadhesion phenomenon under different pH conditions. *Polymers*, **14**(**22**), 4978 (2022) https://doi.org/10.3390/polym14224978

[48] López-López M, Fernández-Delgado A, Moyá ML, Blanco-Arévalo D, Carrera C, de la Haba RR. Optimized preparation of levofloxacin loaded polymeric nanoparticles. *Pharmaceutics*, **11**(**2**), 57 (2019) https://doi.org/10.3390/pharmaceutics11020057

[49] Mohamed S, Nasereldin M, Refai H. Preparation and characterization of terbutaline sulphate loaded chitosan/Carbopol nanoparticles. *J. Adv. Pharm. Res.*, **3**(**1**), 30–4 (2019) https://doi.org/10.21608/APRH.2019.6474.1071

[50] Alhowyan AA, Kalam MA, Iqbal M, Raish M, El-Toni AM, Alkholief M. Mesoporous silica nanoparticles coated with carboxymethyl chitosan for 5-fluorouracil ocular delivery: characterization, in vitro and in vivo studies. *Molecules*, **28**(**3**), 1260 (2023) https://doi.org/10.3390/molecules28031260

[51] Dudhat K, Patel H. Preparation and evaluation of pirfenidone-loaded chitosan nanoparticles for pulmonary delivery in idiopathic pulmonary fibrosis. *Futur. J. Pharm. Sci.*, **8**, 29 (2022) https://doi.org/10.1186/s43094-022-00419-3

[52] Gupta S, Dubey S, Patel SK, Lakra AP, Minz S. Chitosan-coated CMC and Carbopol hydrogel beads for controlled release of metformin in diabetes management. *J. Appl. Pharm. Res.*, **13**(**2**), 73–85 (2025) https://doi.org/10.69857/joapr.v13i2.1006

[53] Chechare DD, Siddaiah M. Formulation and evaluation of mucoadhesive microspheres of metronidazole. *J. Appl. Pharm. Res.*, **12**(**1**), 93–9 (2024) https://doi.org/10.18231/j.joapr.2024.12.1.93.99

[54] Embafrash Berhe H, Tesfay Mezgebo D, Abrha S, Gebremeskel Haile T, Molla F. Extraction, characterization, and evaluation of *Lepidium sativum* Linn. mucilage as a mucoadhesive polymer. *Adv. Pharmacol. Pharm. Sci.*, **2023**(**1**), 5535344 (2023) https://doi.org/10.1155/2023/5535344

[55] Danyuo Y, Ani CJ, Salifu AA, Obayemi JD, Dozie-Nwachukwu S, Obanawu VO, Soboyejo ABO, Soboyejo WO. Anomalous release kinetics of prodigiosin from poly-N-isopropyl-acrylamide based hydrogels for the treatment of triple negative breast cancer. *Sci. Rep.*, **9**, 3862 (2019) https://doi.org/10.1038/s41598-019-39578-4

[56] Sabei FY, Safhi AY, Alsalhi A, Khan KA, Bakkari MA, Al Fatease A, Madkhali OA. Preparation and in vitro evaluation of levofloxacin-loaded floating tablets using various rate-controlling agents. *ACS Omega*, **8**(**45**), 42659–66 (2023) https://doi.org/10.1021/acsomega.3c05419

[57] Lin YS, Tsay RY. Drug release from a spherical matrix: theoretical analysis for a finite dissolution rate affected by geometric shape of dispersed drugs. *Pharmaceutics*, **12**, 582 (2020) https://doi.org/10.3390/pharmaceutics12060582

[58] Uskoković V. Mechanism of formation governs the mechanism of release of antibiotics from calcium phosphate nanopowders and cements in a drug-dependent manner. *J. Mater. Chem. B*, **7**(**25**), 3982–92 (2019) https://doi.org/10.1039/C9TB00444K